Journal of Alloys and Compounds 649 (2015) 67–75

Contents lists available at ScienceDirect

Journal of Alloys and Compounds

journal homepage: http://www.elsevier.com/locate/jalcom

Experimental constraints on gold and silver solubility in iron sulfides

Galina Pal'yanova [a, b], Yuri Mikhlin [c], Konstantin Kokh [a, b, d, *], Nick Karmanov [a], Yurii Seryotkin [a, b]

[a] Institute of Geology and Mineralogy, Siberian Branch of the Russian Academy of Sciences, 3, Koptyuga, Novosibirsk, 630090, Russia
[b] Novosibirsk State University, Russia, 2, Pirogova, Novosibirsk, 630090, Russia
[c] Institute of Chemistry and Chemical Technology, Siberian Branch of the Russian Academy of Sciences, Akademgorodok, 50/24, Krasnoyarsk, 660036, Russia
[d] Siberian Physical–Technical Institute of Tomsk State University, 1, Novosobornaya, Tomsk, 634050, Russia

ARTICLE INFO

Article history:
Received 15 March 2015
Received in revised form
15 July 2015
Accepted 16 July 2015
Available online 21 July 2015

Keywords:
Iron sulfides (pyrite, pyrrhotite, troilite)
Au–Ag sulfides (acanthite, uytenbogaardtite, petrovskaite)
Ag–Au alloys
"Invisible" gold and silver

ABSTRACT

Experiments were performed to determine crystallization of Fe,S-melts (pyritic and troilitic with molar ratio S/Fe ratios of 2 and 1, respectively) containing traces of gold and silver at $(Ag/Au)_{wt}$ ratios varying from 10 to 0.1. The solid products were studied by optical microscopy, scanning electron microscopy, X-ray powder diffraction (XRD), microprobe analysis, and X-ray photoelectron spectroscopy (XPS) in order to reveal the concentration limits of "invisible" gold and silver in magmatic iron sulfides, and to determine the influence of sulfur on forms of precious metals in the Fe–S system with different Ag/Au ratios.

Au–Ag phases do not form inclusions but instead concentrate on the grain boundaries in the synthetic pyrrhotite and troilite, while pyrite comprises micro- (1–5 μm) and macroinclusions of Au–Ag alloys and Au–Ag sulfides. In "pyritic" systems, the fineness of alloys increases from 650 to 970‰ and the composition of sulfides changes from acanthite (Ag_2S) to uytenbogaardtite (Ag_3AuS_2) and petrovskaite (AgAuS) as the Ag/Au ratio decreases. The concentrations of "invisible" precious metals revealed in troilite were 0.040 ± 0.013 wt.% Au and 0.079 ± 0.016 wt.% Ag. Measured concentrations in pyrite and pyrrhotite were <0.024 wt.% Au and <0.030 wt.% Ag. The surface layers of iron sulfides probed with XPS were enriched in the precious metals, and in silver relative to gold, especially in the systems with Fe/S = 1, probably, due to depletion of the metallic alloy surfaces with gold. Au- and Ag-bearing iron sulfides crystallized primarily from melts may be the source of redeposited phases in hydrothermal and hypergene processes.

1. Introduction

Iron sulfides, pyrite (FeS_2), pyrrhotite ($Fe_{1-x}S$) and its stoichiometric end-member troilite (FeS), are common minerals in a wide variety of geological formations including sedimentary deposits, hydrothermal veins, metamorphic and magmatic rocks [1]. The behavior of precious metals in igneous systems is largely controlled by sulfide minerals, and quantitative determination of the abundance of gold and silver in primary iron sulfides can provide key information about the distribution of these elements during various magmatic processes. Iron sulfides can accumulate minor and trace elements, including gold and silver [2–9], however, the state of precious metals is still under discussion [4,10,11]. It is often assumed that gold and silver are presented as discrete metallic gold, silver or Au–Ag alloy particles in pyrite, pyrrhotite and other sulfides [12]. Other authors believe that gold is embedded in the crystal lattice of sulfides forming solid solution (being referred as "invisible", "isostructural", "structurally-bound", "chemically bound", "isomorphic" gold) [13–15]. Bortnikov et al. [16] have established the presence of both native and isomorphic gold in sulfide ores using Mössbauer and photoelectron spectroscopy. The nature of the occurrence, concentration ranges, and the variation in amounts of precious metals in pyrrhotite, pyrite and other sulfides were reviewed by Cabri [5], who demonstrated that the metals occur both as invisible form and as submicroscopic native gold or other minerals inclusions. It has been shown recently that pyrite can host trace elements not only as "structurally bound" species or solid solution, but also as nanoparticles of metals with varying degrees of compositional complexity from native Au to Fe–As–Sb–Pb–Ni–Au–S nanophases [6,17–20]. It has been noted that gold-bearing pyrite is commonly arsenic-bearing, leading to a paradigm that As is essential for Au to enter the pyrite structure.

* Corresponding author.
E-mail address: k.a.kokh@gmail.com (K. Kokh).

http://dx.doi.org/10.1016/j.jallcom.2015.07.131
0925-8388/

The limit of structurally-bound Au accommodated by arsenian pyrite is 0.5 wt.% Au at 10 wt.% As [20,21]; Palenik et al. [20] have determined that Au may be present as discrete nanoparticles of gold (~5–10 nm) in As-rich overgrowths on pyrite from the Screamer deposit in the Carlin trend.

Cook et al. [18] analyzed the range of elements, including Au, Te, Ag, Pb, Bi, Cu, Co, Ni and As, in pyrites from 3 gold deposits in China have shown that As-free pyrite can readily contain significant amounts of invisible gold, both as nanoparticles and as locked in the sulfide lattice. The authors identified the importance of Te and other "low melting point chalcophile elements" (e.g., Bi) in governing the high concentrations of gold. Au-telluride nanoparticles were revealed in "arsenic-free" pyrite from an intrusion-hosted Au deposit with orogenic overprint (Dongping, China) [22]. The results presented in Ref. [7] indicate that most of the Au in pyrite from the Dexing porphyry Cu deposit is contained in solid solution at concentrations <0.001 wt.%, but higher concentrations (e.g., 0.01–0.1 wt.% Au) reported are exclusively related to micro-to nano-sized particles of Au.

Modern surface-sensitive methods provide evidence for the existence of nanometer-sized objects at the surfaces of ore minerals. Gold was found in natural iron sulfides as surface phase [23,24]; also surface-bound gold was found to adsorb onto minerals during the mineralization and subsequent oxidation or metallurgical processing [25].

Magmas play an important role as a source of metals and sulfur for hydrothermal ore deposit formation. During the two last decades a considerable attention has been paid to the investigation of gold and silver behavior in Fe, S-containing melts [26–29]. The sulfide melt acts as a "collector" for gold, silver, platinum, palladium, rhodium, ruthenium, iridium, osmium, and other elements, the contents of which are 10–100,000 times higher than in silicate melts [30]. Zajacz et al. [31] have determined from the solubility of Au, Cu and Ag in pyrrhotite crystallized in silicate melts at 200 MPa, 800–1000 °C. The solubility of silver decreases from 0.034 to 0.040 wt.% (basalt, andesite and dacite melts) at 1000 °C to 0.012 wt.% (rhyolite melt) at 800 °C, while that of gold reaches the values of 0.051–0.059 to 0.002 wt.%, respectively. Maximal concentrations of isomorphous gold soluble in pyrite and pyrrhotite at 450°C and 100 MPa were found to be 0.0025 and 0.0005 wt.%, respectively. Tauson et al. [3,32] reported the solubility of Ag as 0.035–0.15 wt.% and Au as 0.015–0.08 wt.% in pyrrhotite from assemblage with magnetite + immiscible Fe–S–O melt + rhyolite melt at 1050 °C. Yang et al. [8] measured "invisible" gold, silver and other elements contents in primary sulfide minerals from granitoids. Maximum contents of Ag and Au reach 0.0123 and 0.0021 wt.% in pyrite, while those in pyrrhotite are 0.00465 and 0.000034 wt.%, respectively.

In the Fe–S system, $Fe_{1-x}S$ (hexagonal pyrrhotite) is stable at S contents of 36.5–41.2 wt.%, whereas FeS_2 (pyrite, cubic) originates from a peritectic reaction at 743 °C and undergoes a transition to the orthorhombic form (marcasite) at 425 °C. Three nearly stoichiometric superstructure compounds, $Fe_{11}S_{12}$, $Fe_{10}S_{11}$, and Fe_9S_{10}, are known in addition to troilite (FeS) and monoclinic pyrrhotite (Fe_7S_8) at room temperature [33,34]. Available experimental data for the four component Fe–S–Ag–Au system are scarce, and the coupled solubility of gold and silver in iron sulfide melts is poorly studied. It is known that 7 and 4.4 wt.% of gold dissolves in FeS at 1250 and 1200 °C, respectively, while silver solubility approaches 20–25 wt.% at these temperatures [35]. Some authors [36–38] suggested that gold is originally concentrated in early pyrrhorite (at concentrations up to 0.0030 wt.%) with following exsolution during peritectic transformation of the matrix to pyrite-marcasite.

Gold contents reported for natural hydrothermal pyrites vary from 10^{-6} to 10 wt.% [2,3,11,13–15]; concentrations of silver in iron sulfides do not exceed 0.27 wt.% [39]. Up to 0.032 wt.% of "invisible" gold was established in pyrite from modern submarine sulfide ores of the Manus Basin (Pacific Ocean) [16]. According to the review of Cabri [5], the concentration of precious metals varied from 0.006 to 1.8 wt.% in pyrrhotite and from 0.25 to 0.80 wt.% in pyrite. Fleischer [40] has estimated the maximal solubility of Ag and Au in natural pyrites to be 0.02 wt.% while the data of Abraitis et al. [2] show 0.0009–0.09 wt.% for Ag and 0.7 wt.% for Au.

Although invisible silver in iron sulfides has been proven and measured in a number of studies, understanding of silver incorporation in iron sulfides lags well behind that of gold. Huston et al. [41–44] stressed the importance of Ag/Au ratios for ore-forming processes. Investigation of the Au and Ag behavior in the Fe–S system is of fundamental and practical importance both for understanding their occurrence in the pyrite- and pyrrhotite-containing ores, and precious metal extraction from refractory sulfide ores.

In this work we performed the experiments on coupled gold and silver solubility in magmatic iron sulfides (pyrite, troilite, pyrrhotite); the study was confined to the simple Fe–S system with Ag/Au ratios typical for sulfide ores. The aim was to reveal the solubility of gold and silver and to determine the influence of sulfur on visible forms of precious metals in Fe–S system with different Ag/Au and S/Fe ratios. X-ray photoelectron spectroscopy was also applied to characterize the surface layers of the mineral assemblies largely determining their reactivity upon weathering and the mineral processing.

2. Experiments and analytical methods

2.1. Starting compositions

The starting materials were elementary gold and silver (99.99%), sulfur (99.9%) and iron (99.5%). The compositions of chosen samples can be formally written down as $FeS_2Ag_{0.1(or\ 0.01)-x}Au_x$ ("sulfur-rich" or "pyritic" system) and $FeSAg_{0.1(or\ 0.01)-x}Au_x$ ("sulfur-depleted" or "troilitic" system) (x = 0.0035; 0.019; 0.02; 0.056; 0.06; 0.04 or 0.08) (Table 1). Therefore, molar ratio of sulfur to iron (S/Fe) was 2 or 1 and weight ratio $(Ag/Au)_{wt}$ varied from ~10 to ~0.1.

2.2. Experimental method

For each sample the charge and the quartz rod, which was used to minimize the free volume, were loaded into a quartz ampoule. Sealing of the ampoules was performed after evacuating them to a residual pressure of ~10^{-4} torr. To prevent an explosion of the ampoules due to excess sulfur pressure, the mixture was heated for 72 h at a rate of 0.2–0.5°/min. The ampoules (Py1 ÷ Py7, Tr1 ÷ Tr7, Table 1) were heated to 1050 °C for 12 h and then cooled at a rate 0.2°/min to 150 (Py1 ÷ Py4) and 500 °C (Py5, Py6, Tr5, Tr6) and thereafter annealed at this temperature for 30 and 7 days, respectively. At the end of the annealing procedure the furnace was switched off and the ampoules were cooled to room temperature for about 7–10 h. The ampoules Py7, Tr1 ÷ Tr4 and Tr7 were cooled to room temperature for about 24 h without being annealed. The maximal temperature of the experiments ensured a full melting of the samples [34], while the annealing corresponded to conditions of high- and low temperature metamorphic processes.

2.3. Analytical techniques

2.3.1. Electron microprobe analysis

The samples were preliminary studied by optical and scanning electron microscopy (SEM). Polished sections were prepared from 1/3 part of each sample. The chemical composition was determined by energy-dispersive (EDS) and wavelength-dispersive (WDS)

Table 1
The results of electron microprobe (EMPA) and X-ray diffraction (XRD) analyses of the solid phases crystallized in experiments with the starting composition $FeS_2Ag_{0.1(or\ 0.01)-x}Au_x$ ("pyritic" system) and $FeSAg_{0.1(or\ 0.01)-x}Au_x$ ("troilitic" system) (x = 0.0035 ÷ 0.08).

No exp.	Starting composition	$T_{annealing}$/$(Ag/Au)_{wt}$	Synthesized solid phases (fineness of gold, ‰)
"sulfur-rich" system (Fe/S=2)			
Py1	$FeS_2Ag_{0.095}Au_{0.005}$	150 °C/10	Po > Py > Ac + Au,Fe–Ac[a]
Py2	$FeS_2Ag_{0.08}Au_{0.02}$	150 °C/2	Po > Py > Uyt + Fe-Uyt[a] + Au–Ag alloy (750)
Py3	$FeS_2Ag_{0.06}Au_{0.04}$	150 °C/0.75	Po > Py > Uyt + Pet + Au–Ag alloy (930)
Py4	$FeS_2Ag_{0.02}Au_{0.08}$	150 °C/0.125	Po > Py > Pet + Au–Ag alloy (920)
Py5	$FeS_2Ag_{0.081}Au_{0.019}$	500 °C/2.13	Po > Py > Ac + Au–Ag alloy (650)
Py6	$FeS_2Ag_{0.044}Au_{0.056}$	500 °C/0.39	Po > Py > Pet + Au–Ag alloy (970) + S
Py7	$FeS_2Ag_{0.0065}Au_{0.0035}$	No/0.93	Po > Py >> Uyt + Pet + Ag–Au alloy (930)
"sulfur-depleted" system (Fe/S=1)			
Tr1	$FeSAg_{0.095}Au_{0.005}$	No/10	Tr >> Au–Ag alloys (20÷100)
Tr2	$FeSAg_{0.08}Au_{0.02}$	No/2	Tr >> Au–Ag alloys (90÷350)
Tr3	$FeSAg_{0.06}Au_{0.04}$	No/0.75	Tr >> Au–Ag alloys (290÷600)
Tr4	$FeSAg_{0.02}Au_{0.08}$	No/0.125	Tr >> Au–Ag alloys (400÷950)
Tr5	$FeSAg_{0.081}Au_{0.019}$	500 °C/2.13	Tr >> Au–Ag alloys (240÷600)
Tr6	$FeSAg_{0.044}Au_{0.056}$	500 °C/0.39	Tr >> Au–Ag alloys (120÷800)
Tr7	$FeSAg_{0.0065}Au_{0.0035}$	No/0.93	Tr >> Au–Ag alloys (270÷650)

Mineral abbreviations: pyrite Py, pyrrhotite Po, troilite Tr, acanthite Ac, uytenbogaardtite Uyt, petrovskaite Pet.
[a] Iron presents in Au–Ag sulfides.

electron microprobe analysis (EPMA) using a scanning electron microscope MIRA 3 LMU (Tescan Orsay Holding) combined with X-ray microanalysis systems INCA Energy 450+ Xmax-80 and INCA Wave 500 (Oxford Instruments Nanoanalysis Ltd). EDS EPMA was carried out at an accelerating voltage of 20 kV, probe current 1.5 nA, live acquisition time of spectra 30 s. For the analysis we used the Xray K-series (S, Fe) and L-series (Ag, Au). The spatial resolution of the analysis was about 3 μm. Relatively large grains more than 10 μm in size were examined to avoid background fluorescence from surrounding phases. Pure metals (Au and Ag) and pyrite (FeS_2) were used as reference samples. The accuracy of X-ray microprobe analysis was 1.5 rel. % for Au and 1 rel.% for Ag in Au–Ag alloys, and 1 rel.% for Fe and 0.5 rel.% for S in sulfides.

The amount of invisible gold in sulfides was estimated by WDS EPMA using Au M-line at an accelerating voltage of 20 kV, probe current 20 nA, acquisition time of 400 s for peak, and 200 s for background measurement on each side of the peak. The concentration of silver was measured by the Energy-dispersive spectrometer (live acquisition time 570 s). The analyses were made on the 10 × 10 μm^2 areas in a raster mode. The lower limits of detection at the given parameters were estimated as 0.024 wt.% for Au and 0.030 wt.% for Ag.

2.3.2. X-ray powder diffraction (XRD)

X-ray powder diffraction patterns were collected on a Stoe STADI MP diffractometer (CuKα1 radiation, Ge(111)

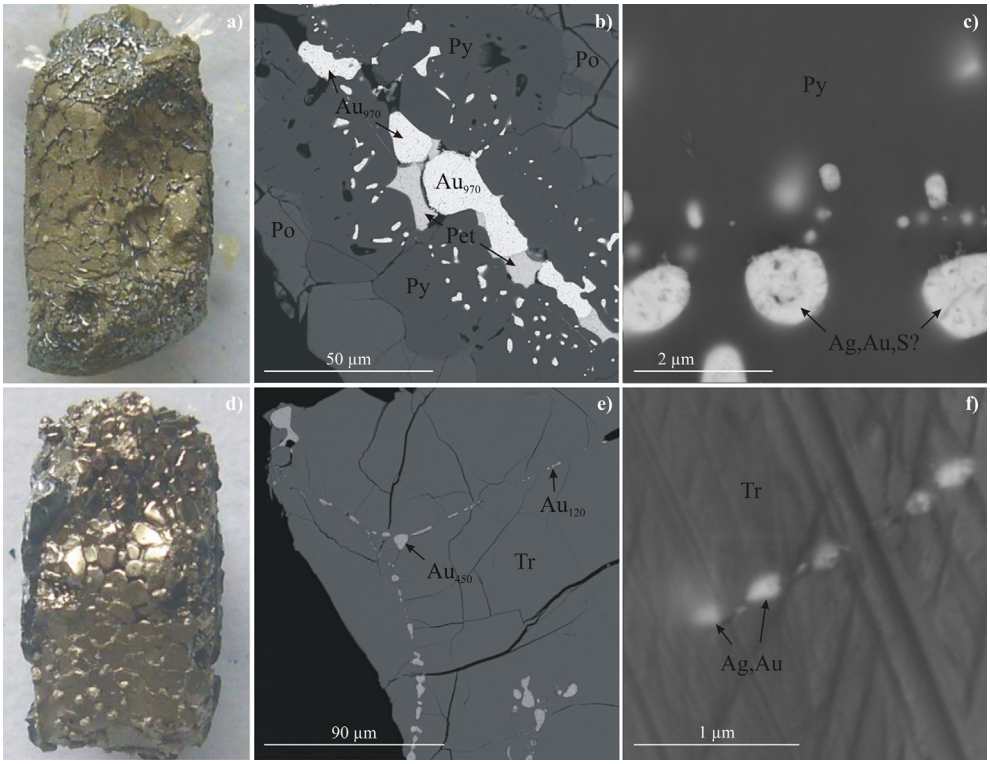

Fig. 1. Optical and SEM photos of pyritic (a,b,c) (Py6) and troilitic (d,e,f) (Tr6) samples. Symbols of the synthesized phases: Py – pyrite. Po – pyrrhotite. Tr – troilite. Pet – petrovskaite. Au_N – Ag–Au alloys and their fineness. Ag, Au,S? – exact composition was not determined due to the small size.

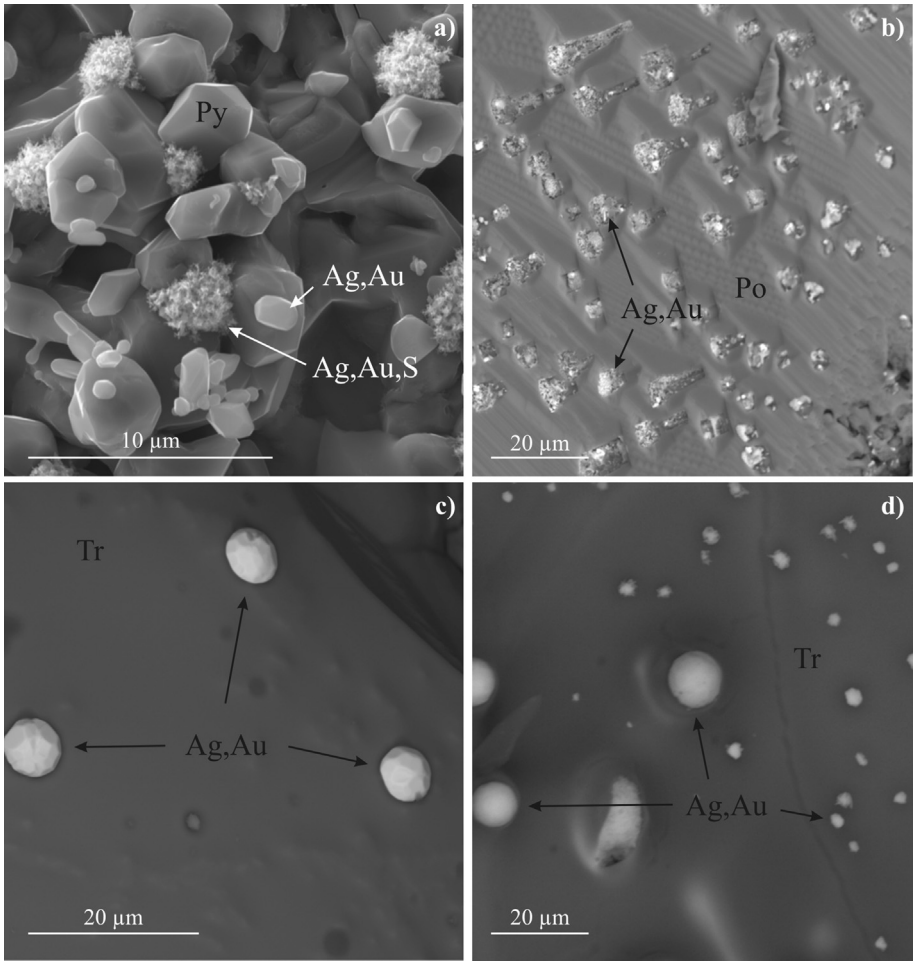

Fig. 2. Microcrystals of Au–Ag alloys and Au–Ag sulfides on the surface of the samples Py6 (a), Py7 (b), Tr6 (c), Tr1 (d).

monochromator, 40 kV, 40 mA) equipped with a MITHEN 1K linear detector. The diffraction data were collected from 15 to 60° 2θ angular range with a step of 0.015° and accumulation time of 15 s per step. The results were processed in the program WinXPOW 2.21 (Stoe). The database of PDF-4 Minerals (The Powder Diffraction File PDF-4 +, 2006) [45] was used for phase specification.

2.3.3. X-ray photoelectron spectra (XPS)

X-ray photoelectron spectroscopy (XPS) experiments were performed on specimens crushed to 100–200 μm in a jasper mortar, immediately attached to a conductive carbon sticky tape and transferred to the vacuum chamber. The measurements were carried out using an SPECS instrument equipped with a hemispherical analyzer PHOIBOS 150 MCD 9 at electron take-off angle 900. The pass energy was set at 8 eV and 20 eV for high resolution narrow scans and for survey spectra, respectively; unmonochromatized Mg Kα radiation (1253.6 eV) of the X-ray tube was used for excitation. The lines were fitted with Gaussian–Lorentzian peak profiles after Shirley background subtraction using CasaXPS software.

3. Results and discussions

The starting compositions and the results of analyses of the solid phases crystallized in the "pyritic» (Py1 ÷ Py7) and "troilitic" (Tr1 ÷ Tr7) experiments are shown in Table 1. Fig. 1 demonstrates the examples of experiments from each series (Py6 and Tr6).

The major phases in «pyritic » experiments are represented by pyrrhotite ($Fe_{0.47}S_{0.53}$ or Fe_7S_8) and pyrite ($Fe_{1.00}S_{2.00}$ or $Fe_{0.99}S_{2.01}$). Pyrrhotite forms large resorbed grains surrounded by fine-grained aggregates of pyrite (Fig. 1b, Py6). Au–Ag sulfides were found in all the samples synthesized in "pyritic" experiments, while Au–Ag alloys appeared only in Py2 – Py7. Micrograins of Au–Ag sulfides and Au–Ag alloys (Fig. 1d, Py6) less than 1–5 μm in size are localized mostly in pyrite along the borders with pyrrhotite. Large xenomorphic grains of Au–Ag sulfides are generally in the central part of pyrite grains. Separate coarse grains of fine gold (5–50 μm) intergrow with Au–Ag sulfides in pyrite crystals (Fig. 1b, Py6). The composition of Au–Ag sulfides and Au–Ag alloys depends on Ag/Au ratios in the initial loading (Table 1), with acanthite Ag_2S ($(Ag/Au)_{wt} = 10 \div 2.13$; experiments Py1, Py5), uytenbogaardtite Ag_3AuS_2 (Ag/Au)wt = 2 ÷ 0.75; experiments Py2, Py3), and petrovskaite AgAuS ($(Ag/Au)_{wt} = 0.93 \div 0.12$; experiments Py3, Py4, Py6, Py7) produced. The presence of iron in Au–Ag sulfides, that is $Ag_{1.6}Au_{0.2}Fe_{0.1}S_{1.1}$ and $Ag_{2.9}Au_{0.9}Fe_{0.1}S_{2.1}$, is observed in experiments Py1 and Py2, respectively. Detailed results on experiments Py1 ÷ Py4 are shown in Ref. [46]. The fineness of gold ($N_{Au} = Au/\Sigma(Au + Ag)\cdot 1000$, ‰) increases from 650 to 750 ($(Ag/Au)_{wt} = 2.13 \div 2$, experiments Py2, Py5) to 920–970 ‰ ($(Ag/Au)_{wt} = 0.93 \div 0.12$, experiments Py4, Py6, Py7) (Table 1). The iron content in Au–Ag alloys varies in the range 0–5.7 wt.%. The iron impurity in Au–Ag sulfides and alloys may be the result of mechanical contamination of iron sulfide particles during polishing. This assumption is confirmed by the analysis of a few gold-silver alloys by TOFSIMS method (device FERA 3, Tescan Orsay Holding),

Table 2
Relative atomic concentrations of the elements on the surface of the synthesized samples crystallized in experiments with the starting composition $FeS_2Ag_{0.1(or\ 0.01)-x}Au_x$ ("pyritic" system) and $FeSAg_{0.1(or\ 0.01)-x}Au_x$ ("troilitic" system) (x = 0.004 ÷ 0.08) (XPS data).

No exp.	Starting composition	$T_{annealing}$ °C	Fe	S	Ag	Au
"sulfur-rich" system						
Py1	$FeS_2Ag_{0.095}Au_{0.005}$	150	1	2.0	0.24	0.011
Py2	$FeS_2Ag_{0.08}Au_{0.02}$	150	1	2.86	0.4	0.057
Py3	$FeS_2Ag_{0.06}Au_{0.04}$	150	1	3.2	0.2	0.08
Py4	$FeS_2Ag_{0.02}Au_{0.08}$	150	1	1.85	0.1	0.081
Py5	$FeS_2Ag_{0.081}Au_{0.019}$	500	1	1.75	0.23	0.005
Py6	$FeS_2Ag_{0.044}Au_{0.056}$	500	1	1.85	0.15	0.09
Py7	$FeS_2Ag_{0.006}Au_{0.004}$	No	1	1.59	0.086	0.002
"sulfur-depleted" system						
Tr1	$FeSAg_{0.095}Au_{0.005}$	No	1	1.27	0.12	Traces
Tr2	$FeSAg_{0.08}Au_{0.02}$	No	1	1.10	0.097	Traces
Tr3	$FeSAg_{0.06}Au_{0.04}$	No	1	0.91	0.065	Traces
Tr4	$FeSAg_{0.02}Au_{0.08}$	No	1	1.43	0.029	Traces
Tr5	$FeSAg_{0.081}Au_{0.019}$	500	1	1.05	0.02	Traces
Tr6	$FeSAg_{0.044}Au_{0.056}$	500	1	1.14	Traces	Traces
	Ar^+ etched	500	1	1.01	Traces	Traces
Tr1	$FeSAg_{0.006}Au_{0.004}$	No	1	1.04	Traces	Traces

indicating an increased iron concentration only in the top layer of the polished particles.

The X-ray diffraction analysis showed that the samples produced in experiments Py1 ÷ Py7 contain cubic pyrite FeS_2 (The Powder Diffraction …, 2006, card 04-004-6511) and monoclinic pyrrhotite Fe_7S_8 (card 00-029-0723). XRD detected acanthite (card 004-008-8450) in the experiment Py1, uytenbogaardtite (card 00-020-0461) (Py2, Py3), and petrovskaite (card 00-019-1146) (Py3, Py4, Py6 and Py7). The samples from experiments Py2 ÷ Py7 comprise a metallic phase with the peaks close to those of silver (card 04-007-7997), gold (card 04-007-8000), and their alloys. Elementary sulfur was observed on the surface of the solid phases (Fig. 1a) or on the ampoule walls in the experiment Py4.

The concentrations of "invisible" precious metals in pyrite and pyrrhotite are lower than the sensitivity limit of X-ray spectral microanalysis (Au < 0.024 and Ag < 0.030 wt.%). "Surface" Au–Ag phases were observed both on pyrite (Fig. 2a) and pyrrhotite (Fig. 2b), in the latter as 1–2 μm species located on crystal vicinals.

Surface compositions determined using XPS are in a qualitative agreement with those for the bulk, except that surface layers are enriched in silver (Table 2). Fig. 3 shows photoelectron Fe 2p, S 2p, Ag 3d and Au 4f spectra and X-ray excited Auger Ag MNN spectra of the samples $FeS_2Ag_{0.1-x}Au_x$ synthesized using different initial compositions (Py1 ÷ Py4, Table 1). Narrow peaks at the binding energy (BE) of 707.2 eV in the spectra of iron are due to low-spin Fe(II) in pyrite; the overlapping bands at higher BEs are attributable to high-spin Fe(II) in pyrrhotite (BEs of 708–709 eV) and Fe(III) in oxyhydroxides (about 710 eV and higher) resulted from the surface oxidation.

The highest intensity of the pyritic iron line was observed for the sample with the largest content of silver. The S $2p_{3/2,1/2}$ spectra are better fitted with three doublets which can be assigned to monosulfide species (S $2p_{3/2}$ at 161.3 eV) in pyrrhotite and Ag–Au sulfides, disulfide ions in FeS_2 (about 162.6 eV), and elementary sulfur and/or polysulfide species (near 164 eV). The relative proportion of monosulfide increases for the samples with increasing content of silver mainly due to growing yield of pyrrhotite, in agreement with the spectra of iron.

The Ag $3d_{5/2}$ peaks for two samples with higher concentration of silver (x_{Au} = 0.005, 0.02) are centered at 368.1–368.15 eV, which is typical for Ag_2S and Ag_3AuS_2 and related solid solutions, in accord with the position of Auger Ag $M_4N_{45}N_{45}$ line at the kinetic energy of 356.6 eV (not in Figures) and the above results. As the concentration of silver decreases, the Ag 3d bands widen and shift to slightly lower BEs, probably owing to the formation of AgAuS.

The quantities of gold found using XPS correlate with the bulk ones (Table 2). The Au $4f_{7/2}$ binding energy of 84.65 eV for the sample with the lowest content of gold (x_{Au} = 0.005) is characteristic of uytenbogaardtite [47], and it shifts to lower values with increasing concentration of gold, reaching 84.2 eV typical for petrovskaite for the sample with x_{Au} = 0.08. Interestingly, the lines of metallic gold (84.0 eV) were absent or very weak for all the samples studied.

Troilite ($Fe_{1.00}S_{1.00}$) and Au–Ag alloys were specified in the "troilitic" samples Tr1 ÷ Tr7. Au–Ag alloys are present as rounded microinclusions at the boundary of troilite grains (Fig. 1e,f); Au–Ag microspheres also were found on the surface of troilite (Fig. 2c,d). The fineness of Au–Ag alloys depends on the starting Ag/Au ratios and increases from 20 to 100 (Tr1) to 400÷950‰ (Tr4). The contents of «invisible » gold and silver in locations beyond the inclusions of the Au–Ag phases are found to be 0.040 ± 0.013 and 0.079 ± 0.016 wt.%, respectively.

According to the results of XRD study, the solid phases synthesized in experiments Tr1 ÷ Tr7 are hexagonal troilite (The Powder Diffraction …, 2006, card 01-075-8712) and silver (card 04-007-7997) and gold (card 04-007-8000) or Au–Ag alloys.

The photoelectron Fe 2p spectra collected from samples prepared in the sulfur-depleted system $FeSAg_{0.1-x}Au_x$ (x_{Au} = 0.005, 0.02, 0.04 and 0.08, Tr1 ÷ Tr4) (Fig. 4) show wide multiplet lines of high-spin Fe(II) bonded sulfur with the Fe $2p_{3/2}$ maximum near 708 eV and those of Fe(III)–O species at 710 eV and higher BEs; a contribution from low-spin ferrous pyritic species (707.2 eV) is low if any. The rather big quantities of ferric oxyhydroxides, which easily formed on pyrrhotite exposed to atmosphere, are in accordance with the spectra of oxygen (not shown in Figures). The band of monosulfide at about 161.4 eV dominates in the S 2p spectra, while disulfide and polysulfide components (about 162.9 eV) are smaller.

The intensity of Ag 3d spectra and atomic S/Ag ratios (Table 2) vary sympathetically with the total content of silver in the samples. The Ag $3d_{5/2}$ binding energy of 368.25 eV is attributable to metallic silver; it slightly shifts towards smaller BEs with decreasing Ag/Au ratio in the bulk, suggesting the formation of silver sulfide phase(s). In contrast to « pyritic » systems, photoelectron spectra of gold are surprisingly weak (Fig. 4d), even after moderate Ar + sputtering, implying that gold is almost absent on the surfaces exposed by crushing regardless of its total content. A very low signal with Au $4f_{7/2}$ at about 84.3 eV may be assigned to Au(I)–S species, in particular, gold dissolved in ferrous sulfide matrix. This contradicts the microprobe analysis data which show notable quantities of gold in alloys (N_{Au} > 400‰) for the sample with xAu = 0.08 (Table 1, Tr4; Fig. 4d). These findings could be rationalized in terms of small surface areas of these rather big metallic particles (Fig. 4), but the intensities of relevant bands of elementary silver are quite high. So, the most likely explanation is that rather thick near-surface layers of the alloys are strongly depleted in gold and enriched in silver.

Texture study of the synthesized samples suggests the sequence of crystallization of Au–Ag phases and iron sulfides, and reveals formation conditions of invisible and native form and sulfides of gold and silver. The first phase solidified in the sulfur-rich system is hexagonal Au, Ag-bearing pyrrhotite. The next stage of solidification is a formation of pyrite by a peritectic reaction between pyrrhotite and liquid. Precious metals, apart from those solved in Fe–S solid phases, crystallize at the final stage forming xenomorphic fine grains of native gold and Au–Ag sulfides in pyrite; this is well seen in Figs. 1b and 5. This assumption is also confirmed by the resorbed surface of pyrrhotite and idiomorphic grains of pyrite in all experiments. A part of the phases with precious metals may appear in the pyrite as a result of peritectic reaction. In this case, the microinclusions of Au–Ag alloys and Au–Ag sulfides captured by primary pyrrhotite are found to be localized in pyrite, marking the former

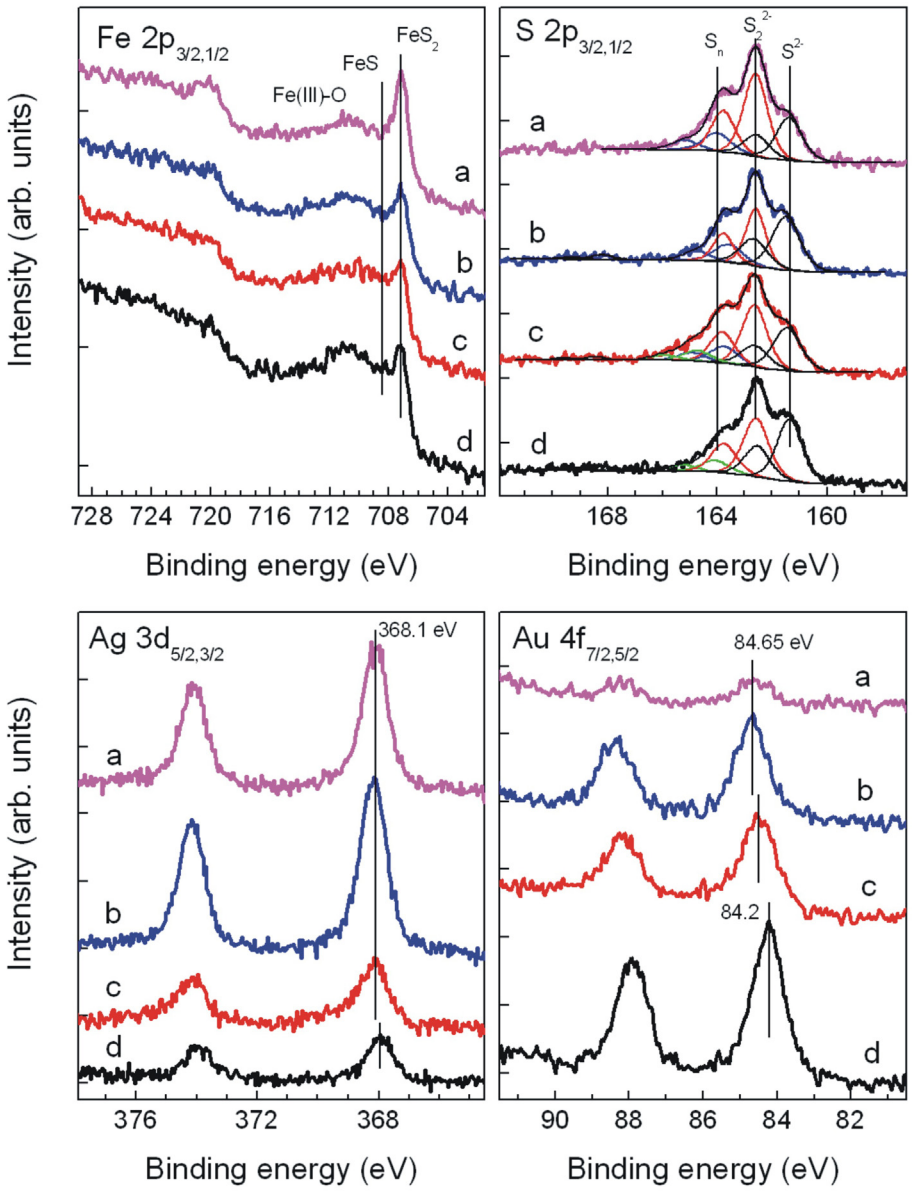

Fig. 3. X-ray photoelectron spectra of $FeS_2Ag_{0.1-x}Au_x$ samples (Py1 ÷ Py4. Table 1) with different initial gold contents: (a) $x = 0.005$. (b) 0.02. (c) 0.04 and (d) 0.08.

boundary of pyrrhotite grains (Fig. 5). A transition of hexagonal pyrrhotite into the monoclinic phase, and solidification of sulfur take place at temperatures 317 and 113 °C, respectively [33]. Transformation of high-temperature polymorphs of Au–Ag sulfides into low temperature ones (α→β) proceeds in the interval of 178–307 °C [48].

The sequence of crystallization of phases in sulfur-depleted system (experiments Tr1 ÷ Tr7, Table 1) is more simple. The first solid formed upon cooling is Au, Ag-containing troilite followed by interstitial crystallization of Au–Ag alloys (Fig. 1e).

Our results on solubility of gold and silver in iron sulfides are in general agreement with those obtained by other authors for experimental [31,32] and natural samples [8,40,41,49–52]. However, the variation of data is possible in the case of complex natural systems; for instance, the presence of copper may be suggested to affect the content of noble metals in massive ores with pyrrhotite from Norilsk-1, Oktyabrsk and Talnakh deposits. The measured concentrations were in the range of 0.000002–0.00026 wt.% for gold and 0.00013–0.0033 wt.% for silver [9,53] which is far lower than average values.

The data obtained here support the model of fractional crystallization of sulfide melts, according to which the precious metals should form their own minerals [30]. The experiments showed that Au–Ag sulfides are quite stable, in addition to the native gold. Recent experimental research [54] also confirms the existence of the sulfide form of gold and silver on the pyrite surface. The phases of $(Au,Ag,Fe)_2S$ composition along with Fe, Cu and Ni sulfides were found in carbonaceous chondrites [55]. The decay structures representing mirmekite-like intergrowths of native gold and uytenbogaardtite in ores of the Original Bullfrog deposit in Canada were diagnosed in Ref. [56]. Native gold – pyrite – acanthite (or uytenbogaardtite) mirmekitic intergrowth was found in the base metal ores of Popsko deposit, Bulgaria [57]. Uytenbogaardtite overgrown by electrum was established in ijolites and nepheline syenites of Goryachegorsk massif [58]. Rare findings of Au–Ag sulfides in the sulfide ores of various genesis are likely to be a result of complicated diagnostics of these minerals caused by their micron sizes and high fragility and low hardness, which lead to their losses

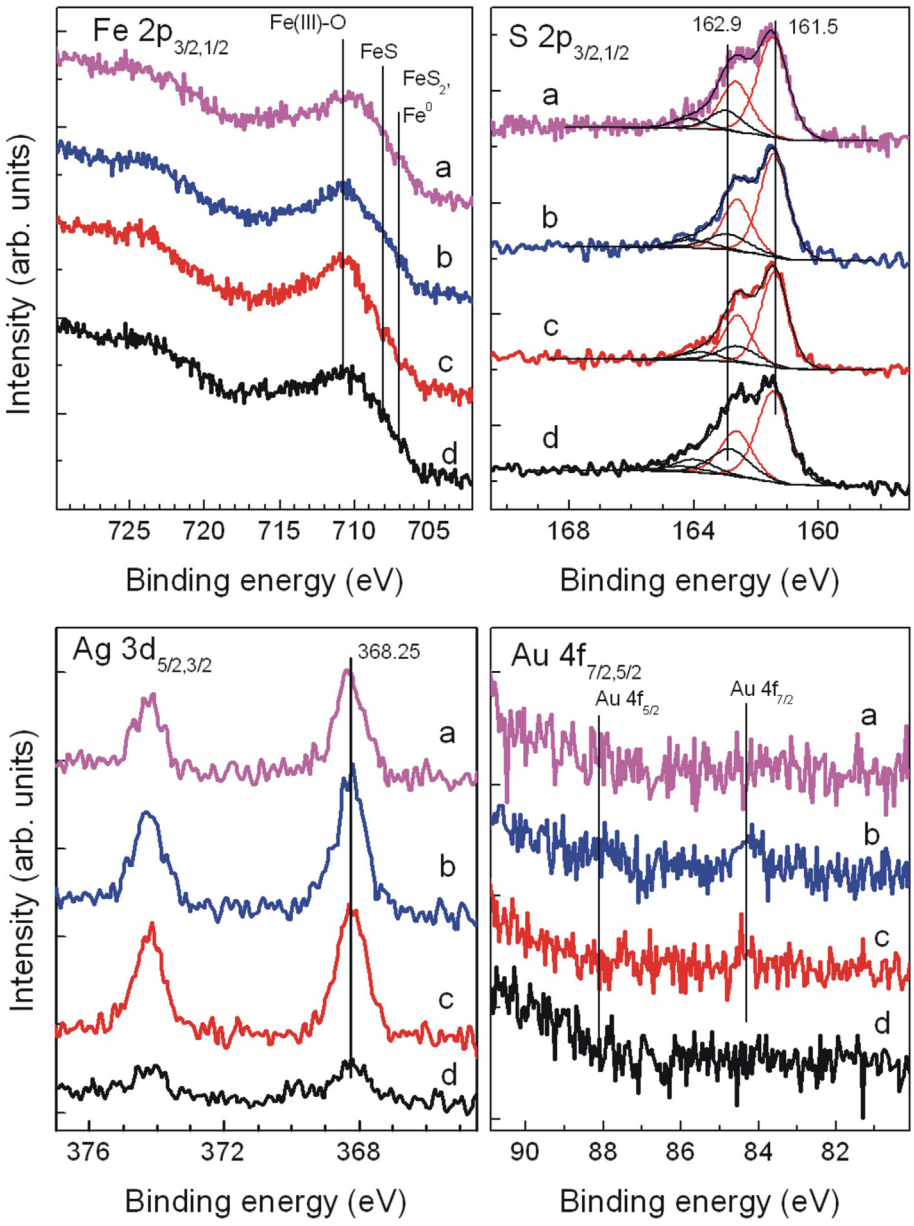

Fig. 4. X-ray photoelectron spectra of $FeSAg_{0.1-x}Au_x$ samples (Tr1 ÷ Tr4. Table 1) with initial gold contents: (a) $x = 0.005$. (b) 0.02. (c) 0.04 and (d) 0.08.

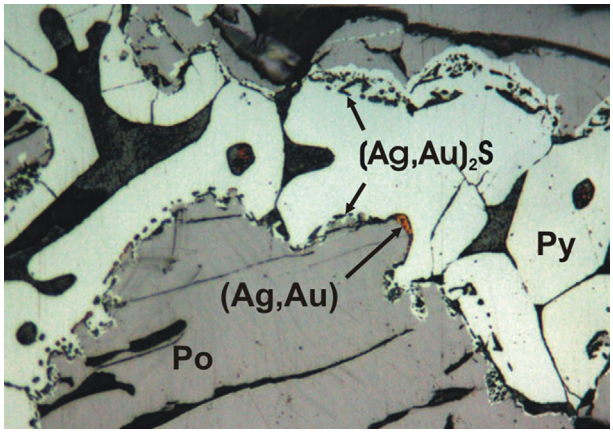

Fig. 5. Microinclusions of Au–Ag alloys and Au–Ag sulfides in pyrite localized near the boundary with pyrrhotite grains (sample Py2).

during fabrication of polished sections, as well as during production of concentrates and schliches [59]. Moreover, "difficult to extract" gold may be connected with the presence of micron-scale inclusions of Au–Ag sulfides in pyrite aggregates. In our opinion, both Au–Ag sulfides and native gold, which crystallize primarily from melts, may be the source of redeposited phases in hydrothermal and hypergene processes [60].

The existing methods for the recovery of precious metals from sulfide ores are focused on native (metallic) form of gold and silver and largely disregard the presence of Au–Ag sulfides – acanthite, uytenbogaardtite and petrovskaite. Data on the solubility of precious metals in iron sulfides are important to balance the various types of gold occurrence in the sulfide ores.

4. Conclusion

1) Crystallization of pyrrhotite and pyrite as major phases occurs in the sulfur-rich system (S/Fe = 2). Precious metals are

concentrated in pyrite as inclusions of alloys and sulfides. With decreasing Ag/Au weight ratio from 10 to 0.1 the fineness of Au alloys increases from 650 to 970‰ and the composition of sulfides changes from acanthite to uytenbogaardtite and petrovskaite. The content of "invisible" precious metals in pyrite and pyrrhotite does not exceed 0.024 and 0.030 wt.% for Au and Ag, respectively.

2) The sulfur depleted system (S/Fe = 1) forms troilite with isomorphous precious metals; their concentrations can reach 0.040 ± 0.013 and 0.079 ± 0.016 wt.% for Au and Ag, respectively. Most of "visible" Au–Ag phases are located between or close to the grain boundaries.
3) The photoelectron spectra characterizing a few nanometer thick layer showed preferentially Ag–Au sulfide phases on the surfaces of ground specimens. Moreover, almost no surface gold was observed in the samples depleted in sulfur ("troilitic"), where the precious metals are present mainly in the elementary form. Probably, the surfaces of metallic Ag–Au alloys are enriched in silver, and the effect being more pronounced in the S-bearing systems due to a higher Ag affinity to S. This may affect the leaching of gold; and it should be taken into consideration for the reactions of weathering and processing of Au-bearing ores.

Acknowledgments

This work is supported by Russian Foundation for Basic Research, grant № 14-05-00504a. The authors thank Dr. Nigel J. Cook for constructive comments and suggestions which greatly improved this manuscript.

References

[1] A.F. Korobeynikov, A.Ya Pshenichkin, Geochemical-peculiarities of pyrite of gold-ore deposits, Geokhimiya 1 (1985) 93–104.
[2] P.K. Abraitis, R.A.D. Pattrick, D.J. Vaughan, Variations in the compositional, textural and electrical properties of natural pyrite: a review, Int. J. Min. Process 74 (2004) 41–59.
[3] V.L. Tauson, S.V. Lipko, Pyrite as a concentrator of gold in laboratory and natural systems: a surface-related effect, in: N. Whitley, P.T. Vinsen (Eds.), Pyrite: Synthesis, Characterization and Uses, Nova Sci. Pub., Inc., NY, 2013, pp. 1–40 (Chapter 1).
[4] D.J. Vaughan, A.R. Lennie, The iron sulphide minerals: their chemistry and role in nature, Sci. Prog. 75 (1991) 371–388.
[5] L.J. Cabri, The distribution of trace precious metals in minerals and mineral products, Mineral. Mag. 56 (1992) 289–308.
[6] A.P. Deditius, M. Reich, S.E. Kesler, S. Utsunomiya, S.L. Chryssoulis, J. Walshe, R.C. Ewing, The coupled geochemistry of Au and As in pyrite from hydrothermal ore deposits, Geochim. Cosmochim. Acta 140 (2014) 644–670.
[7] M. Reich, A. Deditius, S. Chryssoulis, J.-W. Li, C.-Q. Mae, M.A. Parada, F. Barra, F. Mittermayr, Pyrite as a record of hydrothermal fluid evolution in a porphyry copper system: A SIMS/EMPA trace element study, Geochim. Cosmochim. Acta 104 (2013) 42–62.
[8] X.-M. Yang, D.R. Lentz, P.J. Sylvester, Gold contents of sulfide minerals in granitoids from southwestern New Brunswick, Canada, Miner, Deposita 41 (2006) 369–386.
[9] S.J. Barnes, R.A. Cox, M.L. Zientek, Platinum-group element, gold, silver and base Metal distribution in compositionally zoned sulfide droplets from the Medvezky Creek Mine, Noril'sk, Russia, Contrib. Mineral. Petrol 152 (2006) 187–200.
[10] G.K. Czamanske, V.E. Kunilov, M.L. Zientek, L.J. Cabri, A.P. Likhachev, L.C. Calk, R.L. Oscarson, A proton-microprobe study of magmatic sulfide ores from the Noril'sk-Talnakh district, Siberia, Canad, Mineral 30 (1992) 249–287.
[11] V.L. Tauson, A.G. Mironov, N.V. Smagunov, N.G. Bugaeva, V.V. Akimov, Gold in sulfides: state of the art occurrence and horizons of experimental studies, Russ. Geol. Geoph 37 (1996) 1–11.
[12] N.V. Petrovskaya, Gold Nuggets, Nauka, Moscow, 1993, p. 191 [In Russian].
[13] A.G. Mironov, V.F. Geletii, Study of the gold distribution in synthetic pyrites by a radioisotope 195Au, Dokl. USSR 241 (1978) 1428–1431 [In Russian].
[14] N.J. Cook, S.L. Chryssoulis, Concentrations of "invisible gold" in the common sulfides, Canad. Mineral. 28 (1990) 1–16.
[15] J. Besten, D.N. Jamieson, Ch G. Ryan, Lattice location of gold in natural pyrite crystals, Nucl. Inst. Meth. Phys. Res. B 152 (1999) 135–144.
[16] N.S. Bortnikov, L. Cabri, I.V. Vikent'ev, G. McMahon, Yu A. Bogdanov, Invisible gold in sulfides from recent submarine hydrothermal mounds, Dokl. Earth Sci. 373 (2000) 863–866.
[17] A.P. Deditius, S. Utsunomiya, M. Reich, S.E. Kesler, R.C. Ewing, R. Hough, Trace metal nanoparticles in pyrite, Ore Geol. Rev. 42 (2011) 32–46.
[18] N.J. Cook, C.L. Ciobanu, J.W. Mao, Textural control on gold distribution in As-free pyrite from the Dongping, Huangtuliang and Hougou gold deposits, North China Craton, (Hebei Province, China), Chem. Geol. 264 (2009) 101–121.
[19] R. Hough, M. Reich, R. Noble, Noble metal nanoparticles in ore systems, in: Amanda S. Barnard, Haib Guo (Eds.), Nature's Nanostructures, Pan Stanford Publishing Pte. Ltd., 2012, pp. 978–981.
[20] C.S. Palenik, S. Utsunomiya, M. Reich, S.E. Kesler, L. Wang, R.C. Ewing, "Invisible" gold revealed: direct imaging of gold nanoparticles in a Carlin-type deposit, Am. Mineral. 89 (2004) 1359–1366.
[21] M. Reich, S.E. Kesler, S. Utsunomiya, C.S. Palenik, S.L. Chryssoulis, R.C. Ewing, Solubility of gold in arsenian pyrite, Geochim. Cosmochim. Acta 69 (2005) 2781–2796.
[22] C.L. Ciobanu, N.J. Cook, S. Utsunomiya, M. Kogagwa, L. Green, S. Gilbert, B. Wade, Gold-telluride nanoparticles revealed in arsenic-free pyrite, Am. Mineral. 97 (2012) 1515–1518.
[23] V.L. Tauson, R.G. Kravtsova, V.I. Grebenshchikova, E.E. Lustenberg, S.V. Lipko, Surface typochemistry of hydrothermal pyrite: electron spectroscopic and scanning probe microscopic data. II. Natural pyrite, Geochem. Intern. 47 (2009) 231–243.
[24] V.L. Tauson, R.G. Kravtsova, N.V. Smagunov, A.M. Spiridonov, V.I. Grebenshchikova, A.E. Budyak, Structurally and superficially bound gold in pyrite from deposits of different genetic types, Russ. Geol. Geophys. 55 (2014) 273–289.
[25] J. Zhou, B. Jago, C. Martin, Establishing the process mineralogy of gold ores, SGS Miner. Tech. Bull. (2004–03) p1–16.
[26] C. Li, A.J. Naldrett, C.J.A. Coats, P. Johannessen, Platinum, palladium, gold, and copper-rich stringers at the strathcona mine, sudbury – their enrichment by fractionation of a sulfide liquid, Econ. Geol. Bull. Soc. Econ. Geol. 87 (1992) 1584–1598.
[27] M.E. Fleet, M. Liu, J.H. Crocket, Partitioning of trace amounts of highly siderophile elements in the Fe–Ni–S system and their fractionation in nature, Geochim. Cosmochim. Acta 63 (1999) 2611–2622.
[28] J.E. Mungall, D.R.A. Andrews, L.J. Cabri, P.J. Sylvester, M. Tubrett, Partitioning of Cu, Ni, Au, and platinum-group elements between monosulfide solid solution and sulfide melt under controlled oxygen and sulfur fugacities, Geochim. Cosmochim. Acta 69 (2005) 4349–4360.
[29] A.C. Simon, T. Pettke, P.A. Candela, P.M. Piccoli, C.A. Heinrich, The partitioning behavior of As and Au in S-free and S-bearing magmatic assemblages, Geochim. Cosmochim. Acta 71 (2007) 1764–1782.
[30] D.S. Ebel, A.J. Naldrett, Crystallization of sulfide liquids and the interpretation of ore composition, Can. J. Earth Sci. 34 (1997) 352–365.
[31] Z. Zajacz, P.A. Candela, P.M. Piccoli, C. Sanchez-Valle, M. Walle, Solubility and partitioning behavior of Au, Cu, Ag and reduced S in magmas, Geochimica Cosmochimica Acta 112 (2013) 288–304.
[32] A.C. Simon, P.A. Candela, P.M. Picccoli, M. Mengason, L. Englander, The effect of crystal-melt partitioning on the budgets of Cu, Au, and Ag, Am. Mineralogist 93 (2008) 1437–1448.
[33] P. Waldner, A.D. Pelton, Thermodynamic modeling of the Fe-S system, J. Phase Equilib. Diff. 26 (2005) 23–38.
[34] H. Wang, I. Salveson, A review on the mineral chemistry of the non-stoichiometric iron sulphide, $Fe_{1-x}S$ ($0 \leq x \leq 0.125$): polymorphs, phase relations and transitions, electronic and magnetic structures, Phase Transitions 78 (2005) 547–567.
[35] A.E. Guriev, M.B. Tsalikova, On the patterns of distribution of gold and silver between the products of lead melting, Izv. Vyssh. Uchebn. Zaved. Tsvetn. Metall. 2 (1967) 31–40 [In Russian].
[36] A.E. Guriev, M.B. Tsalikova, On the solubility of gold and silver in sufide melts, Izv. Vyssh. Uchebn. Zaved. Tsvetn. Metall. 5 (1967) 59–63 [In Russian].
[37] S.G. Rybkin, Yu L. Nikolaev, V.G. Barankevich, Isothermal Sections at 1473 K through the Pb–Au–FeS and Pb–Ag–FeS phase diagrams, Russ. J. Inorg. Chem. 51 (2006) 470–473.
[38] P. Picot, E. Marcoux, Nouvelles donnees surla metallogenie de l'or, C. R. Acad. Sci. Paris (1987) 221–226, 304, ser. II.
[39] L.A. Taylor, The system Ag-Fe-S: phase equilibria and mineral assemblages, Mineral. Deposita 5 (1970) 41–58.
[40] M. Fleischer, Minor elements in some sulphide minerals, Econ. Geol. 50th Anniv. V. (1955) 970–1024.
[41] D.L. Huston, R.S. Bottrill, R.A. Creelman, K. Zaw, T.R. Ramsden, Geological and geochemical controls on the mineralogy and grain size of gold-bearing phases, eastern Australian volcanic-hosted massive sulphide deposits, Econ. Geol. 87 (1992) 542–563.
[42] C.H. Gammons, A.E. Williams-Jones, Hydrothermal geochemistry of electrum: thermodynamic constraints, Econ. Geol. 90 (1995) 420–432.
[43] G. Pal'yanova, Physicochemical modeling of the coupled behavior of gold and silver in hydrothermal processes: gold fineness, Au/Ag ratios and their possible implications, Chem. Geol. 255 (2008) 399–413.
[44] Y. Liang, K. Hoshino, Thermodynamic calculations of Au_xAg_{1-x} – fluid equilibria and their applications for ore-forming conditions, Appl. Geochem. 52 (2015) 109–117.
[45] The Powder Diffraction File PDF-4+, International Centre for Diffraction Data (ICDD), 2006. Release.
[46] G.A. Pal'yanova, K.A. Kokh, Yu V. Seryotkin, Formation of gold-silver sulfides

and native gold in Fe-Ag-Au-S system, Rus. Geol. Geophys. 53 (2012) 321–329.
[47] Yu L. Mikhlin, V.A. Nasluzov, A.S. Romanchenko, A.M. Shor, G.A. Pal'yanova, XPS and DFT studies of the electronic structures of AgAuS and Ag_3AuS_2, J. Alloys Compd. 617 (2014) 314–321.
[48] M.D. Barton, The Ag–Au–S system, Econ. Geol. 75 (1980) 303–316.
[49] R. Pina, F. Gervilla, S.-J. Barnes, L. Ortega, R. Lunar, Distribution of platinum-group and chalcophile elements in the Aguablanca Ni–Cu sulfide deposit (SW Spain): evidence from a LA-ICP-MS study, Chem. Geol. 302–303 (2012) 61–75.
[50] J.-P. Lorand, O. Alard, Pyrite tracks assimilation of crustal sulfur in Pyrenean peridotites, Min. Petrol 101 (2011) 115–128.
[51] H.V. Thomas, R.R. Large, S.W. Bull, V.V. Maslennikov, R.F. Berry, R. Fraser, S. Froud, R. Moye, Pyrite and pyrrhotite textures and composition in sediments, laminated quartz veins, and reefs at bendigo gold mine, Australia: insights for ore genesis, Econ. Geol. 106 (2011) 1–31.
[52] P. Hazarika, B. Mishra, S.S. Chinnasamy, H.J. Bernhardt, Multi-stage growth and invisible gold distribution in pyrite from the Kundarkocha sediment-hosted gold deposit, eastern India, Ore Geol. Rev. 55 (2013) 134–145.
[53] S.F. Sluzhenikin, A.V. Mokhov, Gold and silver in PGE–Cu–Ni and PGE ores of the Noril'sk deposits, Russ. Miner. Deposita 50 (2015) 465–492.
[54] Yu Mikhlin, A. Romanchenko, M. Likhatski, A. Karacharov, S. Erenburg, S. Trubina, Understanding the initial stages of precious metals precipitation: nanoscale metallic and sulfidic species of gold and silver on pyrite surfaces, Ore Geol. Rev. 42 (2011) 47–54.
[55] T. Geiger, A. Bischoff, Formation of opaque minerals in CK chondrites, Planet. Space Sci. 43 (1995) 485–498.
[56] S.B. Castor, J.J. Sjoberg, Uytenbogaardtite, Ag_3AuS_2, in the Bullfrog mining district, Nevada, Can. Mineral. 31 (1993) 89–98.
[57] V. Mladenova, T. Kerestedjian, A case pyrite-kustelite intergrowth in Popsko deposit, Eastern Rodopes, Bulg. Acad. Sci. – Geochem. Mineral. Petrol. 32 (1997) 29–33.
[58] A.M. Sazonov, E.A. Zvyagina, S.I. Leontiev, M.V. Wolf, T.V. Poleva, V.S. Chekushin, N.V. Oleinikova, Associations of micro- and nano- sized aggregates of precious metals in ores, J. Sib. Fed. Univ. Eng. Techn. 1 (2008) 17–32 [in Russian].
[59] V.P. Samusikov, I.Ya Nekrasov, N.V. Leskova, Gold-silver sulfoselenide $(AgAu)_2(S,Se)$ from the Yakutskoe deposit, Zap. Vses. Mineral. Obshestva 6 (2002) 61–64 [in Russian].
[60] G. Palyanova, N. Karmanov, N. Savva, Sulfidation of native gold, Am. Mineral. 99 (2014) 1095–1103.